nature chemistry

ARTICLES

PUBLISHED ONLINE: 5 OCTOBER 2015 | DOI: 10.1038/NCHEM.2359

Molecular hydrogen interacts more strongly when rotationally excited at low temperatures leading to faster reactions

Yuval Shagam[1], Ayelet Klein[1], Wojciech Skomorowski[2], Renjie Yun[3], Vitali Averbukh[3], Christiane P. Koch[2] and Edvardas Narevicius[1]*

The role of internal molecular degrees of freedom, such as rotation, has scarcely been explored experimentally in low-energy collisions despite their significance to cold and ultracold chemistry. Particularly important to astrochemistry is the case of the most abundant molecule in interstellar space, hydrogen, for which two spin isomers have been detected, one of which exists in its rotational ground state whereas the other is rotationally excited. Here we demonstrate that quantization of molecular rotation plays a key role in cold reaction dynamics, where rotationally excited *ortho*-hydrogen reacts faster due to a stronger long-range attraction. We observe rotational state-dependent non-Arrhenius universal scaling laws in chemi-ionization reactions of *para*-H_2 and *ortho*-H_2 by He(2^3P_2), spanning three orders of magnitude in temperature. Different scaling laws serve as a sensitive gauge that enables us to directly determine the exact nature of the long-range intermolecular interactions. Our results show that the quantum state of the molecular rotor determines whether or not anisotropic long-range interactions dominate cold collisions.

The hydrogen molecule is the most abundant molecule in interstellar space and participates in many reactions of astrochemical relevance[1]. At low temperatures of several kelvins up to several tens of kelvins (typical to the interstellar medium), hydrogen can be found in two quantum states: nuclear spin anti-symmetric *para*-hydrogen, which remains in the rotational ground state, and the symmetric *ortho*-hydrogen, which is rotationally excited. The ratio between *para*- and *ortho*-hydrogen is an important parameter used to estimate the age of interstellar clouds[2,3]. It is thus critical to understand the dependence of inelastic and reactive processes on the internal rotational molecular quantum state.

At low temperatures of a few kelvins, fast barrierless reactions dominate the chemistry of interstellar space[4–6]. In the absence of an activation barrier, the rate-limiting part of the interaction potential shifts from the transition state, which is usually located at the reactants' shortest separation, to the long-range part of the interaction potential. As a result, the conventional Arrhenius law for the dependence of the reaction rate with temperature is replaced by universal scaling power laws[7] as first derived by Paul Langevin in 1905[8]. In his pioneering work, Langevin treated ion and structureless atom collisions. For molecules, however, the long-range interaction is orientation-dependent.

The effect of molecular rotation in fast low-temperature reactions has been studied in the past, but understanding is limited. It was studied theoretically by Clary[5] and Troe[9] and colleagues, and the case of H_2 molecule/ion reactions has been recently addressed by Dashevskaya and co-authors[10]. Additionally, rotational state-selective quenching rates have been experimentally studied by Olkhov and Smith[11] at room temperature. However, experimental evidence of the role of the rotational quantum state of molecules in cold collisions has been entirely missing so far[4].

In the experiments described here, we are able to measure the universal scaling of rotational state-selected reaction rates over a wide range of energies reaching sub-kelvin temperatures. The observed power law serves as a force gauge revealing the exact nature of the long-range interactions that govern collisions for a particular quantum level of the molecular rotor. Here we show that the rotational state of the molecule plays a central role in cold reactions by modifying the long-range forces that are responsible for the reactants' capture at low temperatures. Contrary to the high-temperature regime, where the rotational state of the hydrogen molecule has no influence on the total measured reaction rate, at temperatures of several kelvins, rotationally ground-state and excited-state hydrogen molecules behave as distinct chemical species with different reaction rates.

Some of the prospects of controlling the long-range dominated reactions have been demonstrated by selecting the reactive channel via exchange statistics[12] or electrostatic filtering of molecular conformers that have different dipole moments[13]. In our case, because molecular hydrogen possesses a quadrupole moment, we are able to demonstrate that the contribution of the purely anisotropic, orientation-dependent quadrupole–quadrupole interaction with an open-shell atom depends on the rotational state of the hydrogen molecule. When the molecule is in the ground rotational state, which has an isotropic spatial distribution of the nuclei, only interactions with an isotropic component such as van der Waals can contribute, while the purely anisotropic interactions average to zero. However, if the molecule is in an excited rotational state, the spatial distribution of the nuclei is no longer isotropic, and anisotropic interactions start playing a central role in the reaction dynamics. The quadrupole–quadrupole interaction scales as R^{-5}, while the van der Waals attraction scales as R^{-6}, so its strength overcomes the van der Waals contribution at the large separations that are most relevant to single-digit kelvin temperature range reactions. At these temperatures, the stronger long-range interaction for rotationally excited molecules leads to a dramatic increase in the reaction rate as well as a change in the universal Langevin scaling

[1]Department of Chemical Physics, Weizmann Institute of Science, Rehovot 76100, Israel. [2]Theoretische Physik, Universität Kassel, Heinrich-Plett-Straße 40, Kassel 34132, Germany. [3]Department of Physics, Imperial College London, South Kensington Campus, London SW7 2AZ, UK. *e-mail: edn@weizmann.ac.il

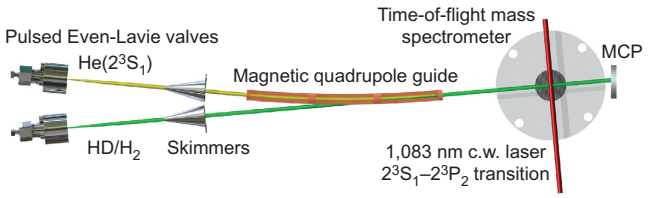

Figure 1 | Schematic of the experimental set-up. Two pulsed Even–Lavie valves, with a 10° angle between them, entrain HD/H_2 (green) and He (yellow) in supersonic beams. The He beam is excited to the 2^3S_1 metastable state and then merged by a magnetic quadrupole guide with the straight HD/H_2 beam. The metastable helium in the low-field-seeking $m = 1$ state collides with the HD/H_2 beam in the time-of-flight mass spectrometer (TOF-MS). To measure the reaction rate with He(2^3P_2), the TOF-MS collection volume is illuminated with a 1,083 nm continuous-wave (c.w.) laser (red) locked onto the transition with a saturated absorption spectroscopy set-up on a helium discharge cell. This produces a 1:1 population distribution between the 2^3S_1 and 2^3P_2 states. The He(2^3S_1) beam is detected with a microchannel plate (MCP) positioned behind the TOF-MS in-line with the beam.

from the $T^{1/6}$ that describes van der Waals long-range interactions to $T^{1/10}$, corresponding to quadrupole–quadrupole interactions[7]. Our result is not limited to a particular collision partner of molecular hydrogen, and the reaction rates at low temperatures will be different for *para*- and *ortho*-hydrogen every time purely anisotropic forces are at play.

Langevin's theory predicts the universal scaling laws of reaction rates, $k_n \propto E^{(n-4)/2n}$, as a function of the collision energy E, where n describes the scaling of the long-range interaction strength with intermolecular separation[7]. To date, some of these universal scaling laws have only been observed in ion-neutral reactions over a limited range of discrete energies between 8 K and 200 K in CRESU (Cinétique de Réaction en Ecoulement Supersonique Uniforme) experiments[14,15]. These measurements of absolute reaction rates revealed the equivalent thermal rate scaling laws $k^2 \propto T^{-1/2}$ in the case of ion–dipole interactions and that k_4 is independent of the collision temperature in the case of ion-induced-dipole interactions. For neutral reactants, inelastic and reactive molecular collisions with near unit probability have been observed at ultracold temperatures[12,16–19], but the direct observation of how the internal molecular degrees of freedom affect the universal scaling has so far eluded experimental investigation. The difficulty has been to experimentally access both the warm and cold reaction regime below the several kelvins needed to distinguish between the low fractional power-law scalings that are characteristic of neutral reactants. Recently, in the case of permanent-induced dipole interactions, the reaction rate of He(2^3S_1) + NH_3 was found to be approximately proportional to $E^{1/6}$ (ref. 20).

Only recently have experiments that span many orders of magnitude in collision energies, extending into the cold regime, been realized. Such methods, which perform collisions with merged supersonic molecular beams in the moving frame of reference, enable continuous tuning of the collision energy from hundreds of degrees kelvin down to 10 mK (refs 21,22). In a different implementation of the same idea, two beams have been merged with separate magnetic and electrostatic guides, leading to cold reactions[20,23]. In the method used here, one beam is magnetically aligned with a second unmanipulated beam[21,22,24], as shown in Fig. 1. So far, these merged beam experiments have been used to study chemi-ionization reactions such as Penning ionization[25], where one reactant is ionized upon collision with a second internally excited reactant. Examples of such reactions, which have attracted interest in astrophysical studies[26], include $He(2^3S_1) + H_2/HD \rightarrow He + e^- + H_2^+/HD^+$. In these reactions, strong shape resonances have been observed, emerging as sharp peaks in the reaction rate[21,24]. The observation of sharp resonance structures indicates that these reactions strongly deviate from the universal limit. Indeed, in the case of He(2^3S_1) collisions with H_2, less than 1% of collisions are reactive at a collision energy of 1 K. These resonances have also been predicted to be sensitive to the rotational state of molecular hydrogen in collisions with F by Alexander and colleagues[27]. In Penning ionization, the electron transfer rate that is responsible for the ionization step is exponentially dependent on atom–molecule separation, as shown in Fig. 3. The repulsive short range interaction between He(2^3S_1) and H_2 leads to a separation larger than $9a_0$ (a_0 is the Bohr radius) between the colliding particles at the position of the inner classical turning point at near-threshold energies (Fig. 2a). When the separation is so large, ionization is suppressed, explaining the observation of the low total ionization rate along with the shape resonances.

However, we can dramatically modify the short-range behaviour of the interaction potential without affecting the ionization width appreciably by exciting the 2^3S_1 metastable helium to the 2^3P_2 state (Fig. 3). In the 2^3P_2 state, helium possesses a quadrupole moment, leading to a strong anisotropy in the interaction potential. Depending on the relative orientation of the H_2 molecule and the $2p$ occupied orbital of He(2^3P_2), the interaction may result in either a strongly repulsive 'wall' or an attractive well with a depth exceeding 5,000 K at short range (Fig. 2b). As the atom–molecule separation decreases, the anisotropy increases. When the anisotropy is on the order of the rotational level spacing of the molecule, it becomes strong enough to reorient the reactants to the most attractive configuration[28,29] and the 'event horizon' or point of no return is reached (Supplementary Section, 'Interaction details'). The reorientation shifts the classical turning point to less than $3a_0$, compared with more than $9a_0$ for the isotropic potential for H_2 with both states of helium, leading to an increase of more than four orders of magnitude in the total ionization width (Fig. 3). Thus, the overall probability for a reaction to occur once the centrifugal barrier is overcome increases to unity as the reactants are inevitably pulled towards each other into a 'black hole' from which they will only emerge after reacting.

Results and discussion

The total He(2^3P_2) + *para*/*ortho*-H_2 reaction rates obtained experimentally, including both the Penning and associative ionization channel products, are shown in Fig. 4. The products of these channels include H_2^+ and HeH^+, with weights of 90 and 10%, respectively for all the collision energies observed. In both cases the rate for He(2^3P_2) is more than two orders of magnitude faster than for He(2^3S_1), indicating the dramatic increase in reaction probability at short separations driven by the strong anisotropy[21,24]. In fact, the total reaction probability P is higher than 99% once the reactants are in the most attractive orientation, calculated according to the classical approximation[25], $P = 1 - \exp[-2\int_{R_c}^{\infty} \Gamma(R)\,dR\sqrt{(\mu/2(E - V(R)))}]$, where R_c is the classical turning point, $\Gamma(R)$ the ionization width, μ is the reduced mass and $V(R)$ is the interaction potential.

Because the reaction takes place regardless of the complicated details that exist within the 'event horizon', only the long-range part of the potential is needed to describe the reaction. Similarly, it has been shown that inelastic rotational and spin–orbit scattering can be described using the details of *ab initio* calculated long-range non-adiabatic interactions[30]. The picture is further simplified because the anisotropy is not strong enough to reorient the reactants at long separations and an averaged, effective long-range potential emerges. Kotochigova and colleagues predicted that such averaging can give rise to an isotropic van der Waals interaction at long range in the universal limit, for ultracold Li + LiYb interactions, which are strongly anisotropic at short range[31]. In the case of He(2^3P_2) + H_2, the long-range interaction is characterized mainly by the van der Waals

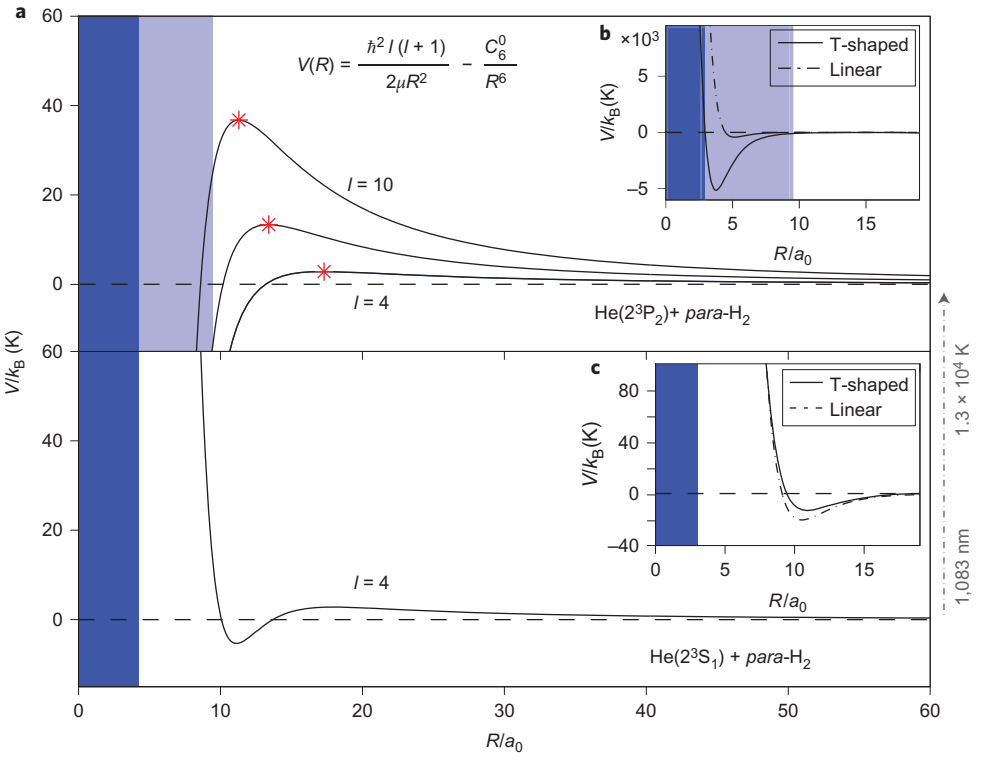

Figure 2 | Interaction potential energy surfaces. a, Interplay between the centrifugal repulsion and the van der Waals attraction forms a barrier at long range in He(2^3P_2) + *para*-H_2 for $l = 4$, 7, 10, where l is the partial wave of the collision and $C_6^0 = 122$ a.u. (black curves, top panel). The isotropic potential energy surface of He(2^3S_1) + *para*-H_2 for $l = 4$ is depicted by the black curve in the bottom panel[24]. **b**, The potential strongly depends on the orientation between the 2*p* occupied orbital of He(2^3P_2) and the molecule, changing the interaction from repulsive to strongly attractive as depicted for the T-shaped ($^3B_2$) and linear ($^3\Pi$) orientations of the molecule. At the 'event horizon' below ~$9a_0$ (depicted by the light-blue shaded region) for the He(2^3P_2) case, the anisotropy becomes strong enough to reorient the reactants to the most attractive orientation, shifting the classical turning point to less than $3a_0$. **c**, On the other hand, the anisotropy for the same two molecular orientations with respect to He(2^3S_1) is not strong enough to reorient the molecule at any separation. The dark-blue shaded region depicts the reaction 'black hole' where the probability for a reaction to occur approaches unity and from which the reactants will only emerge after reacting.

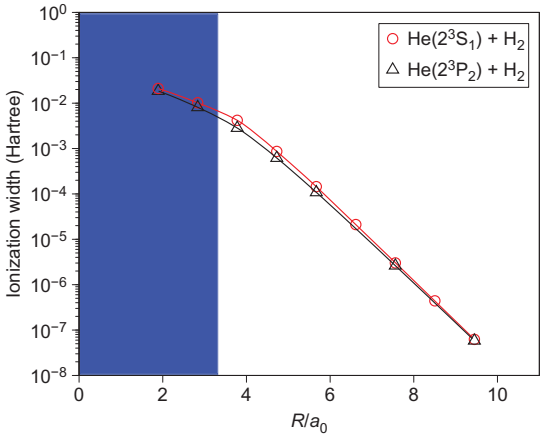

Figure 3 | Penning ionization widths. The ionization widths of H_2 by He(2^3S_1) (red) and He(2^3P_2) (black) increase exponentially as the separation decreases. At short separations the probability reaches the unitary limit at the 'black hole' (blue region) where the reaction will occur with near unit probability.

attraction, which scales as R^{-6}, and the quadrupole–quadrupole interaction, with a different scaling of R^{-5}. The specific type of the effective long-range potential is determined by the rotational quantum state of the molecule, which governs how anisotropy can come into play. Molecular hydrogen formed in the supersonic expansion consists of 75% *ortho*-H_2 and 25% *para*-H_2. Due to the fermionic nuclei statistics, the lowest rotational state of *para*-H_2 is $j = 0$, where j is the molecular rotation quantum number, whereas the lowest rotational state of *ortho*-H_2 corresponds to the first excited state, $j = 1$. To measure the reaction rate of *para*-H_2 we produced pure *para*-H_2 by liquefying *normal*-hydrogen in the presence of a catalyser (see Methods). The rate of *ortho*-H_2 was determined by subtracting the *para*-H_2 contribution from the *normal*-H_2 measurements according to $k_{ortho} = (4/3)(k_{normal} - (1/4)k_{para})$.

When the molecule is in the ground rotational state, $j = 0$, such as in the case of *para*-H_2, the quadrupole–quadrupole interaction, which is purely anisotropic[32], is averaged out at long-range because the distribution of the molecule's nuclei is isotropic. This leads to a reaction rate dominated by the higher-order van der Waals interaction, whose scaling law was first derived by Gorin[7,33] and is written explicitly as

$$k_6(E) = \frac{3\pi}{\sqrt{\mu}}(C_6^{eff})^{1/3}\left(\frac{E}{2}\right)^{1/6} \quad (1)$$

where the reaction rate is defined as $k_n(E) = \sqrt{2E/\mu}\,\sigma_n(E)$, in which σ is the total cross-section and C_6^{eff} is the effective van der Waals interaction strength, which in this case equals our estimated isotropic coefficient $C_6^0 = 122$ a.u. The observed rate of the He(2^3P_2) + *para*-H_2 reaction follows this theoretical universal absolute rate with the $E^{1/6}$ scaling law over more than two orders of magnitude of collision energies down to 0.8 K (Fig. 4a, dashed red line). Below 0.8 K, the reaction rate deviates from the unitary limit, eventually slowing by more than 50% at the lowest collision energies.

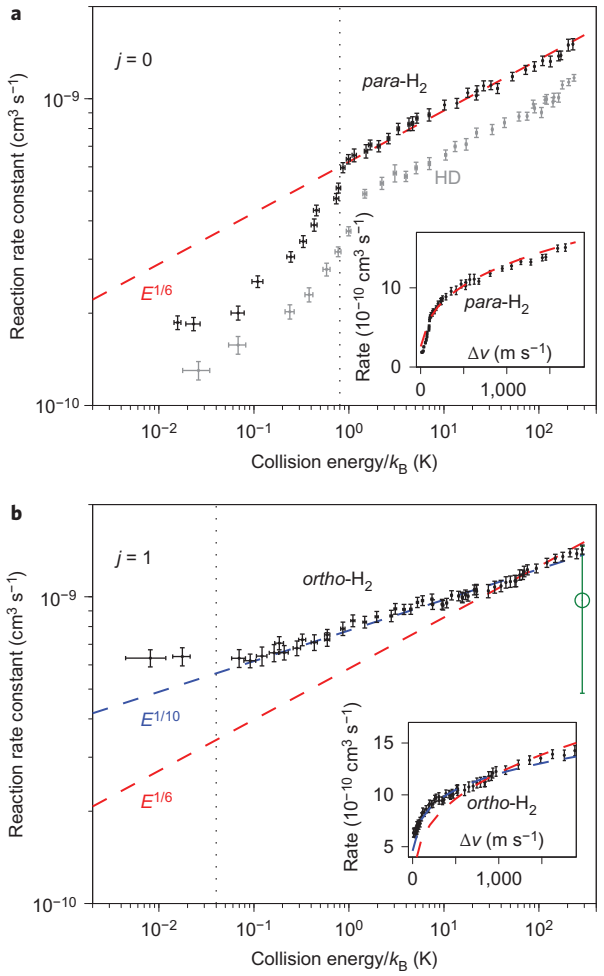

Figure 4 | Reaction rate constants for molecules in excited and ground rotational states with He(2^3P_2) from 10 mK up to 300 K. a, The reaction rate constant with *para*-H_2($j = 0$) follows the theoretical universal Langevin prediction (equation (1) where $C_6^{eff} = C_6^0 = 122$ a.u.) with the $E^{1/6}$ scaling law (red dashed line) down to 0.8 K where the reaction probability drops below unity as indicated by the dashed vertical line. The behaviour is nearly identical for HD($j = 0$), which is shown in arbitrary units (grey symbols). **b**, The reaction rate constant with the rotationally excited *ortho*-H_2($j = 1$) is within the standard deviation of the *para*-H_2($j = 0$) results and is consistent with the $E^{1/6}$ scaling law of the van der Waals interaction (equation (1) where $C_6^{eff} = 100$ a.u.; red dashed line) down to ~30 K before strongly deviating from it. The rate of *ortho*-H_2 follows the $E^{1/10}$ scaling law (equation (2) where $C_5^{eff} = 10.5$ a.u.; blue dashed line) of the quadrupole–quadrupole interaction and becomes clearly distinguishable from other scaling laws at colder temperatures. The green error bar depicts the systematic normalization error[34]. Below the p-wave barrier at 0.04 K (dashed vertical line) the rate assumes a constant value consistent with the Wigner threshold laws. The linear scale insets in **a** and **b** show the rates as a function of the relative mean velocity Δv between the beams, emphasizing the slow deviation from the $E^{1/6}$ scaling (dashed red) in the case of *ortho*-H_2. Error bars represent the standard error of 250–500 measurements at high and low collision energies, respectively. The rate with *ortho*-H_2 is determined by subtracting the contribution of *para*-H_2 from the measurements with *normal*-H_2.

The rate for the He(2^3P_2) + *ortho*-H_2 reaction down to ~30 K is within the standard deviation of the He(2^3P_2) + *para*-H_2 results, consistent with the scaling law $E^{1/6}$ where $C_6^{eff} = 100$ a.u. for *ortho*-H_2, as shown in Fig. 4b (dashed red line). Because *ortho*-H_2 is in the $j = 1$ rotational state, the contributions of the anisotropic components of the interaction are no longer zero and they emerge in the effective long-range potential. These contributions can account for the difference in effective strengths of the van der Waals interaction between *ortho*-H_2 and *para*-H_2. Below ~30 K the difference in reaction rates of *ortho*-H_2 and *para*-H_2 becomes evident. The deviation from the van der Waals scaling law at low energies occurs because the purely anisotropic quadrupole–quadrupole interaction, which was averaged out for *para*-H_2, where $j = 0$, is the leading order term in the effective long-range potential for the $j = 1$ state and now dominates at the lower collision energies. This leads to a reaction rate that scales as $E^{1/10}$ and is explicitly given by

$$k_5(E) = \frac{5\pi}{3^{3/5}\sqrt{\mu}}(C_5^{eff})^{2/5}(2E)^{1/10} \quad (2)$$

where C_5^{eff} is the effective quadrupole–quadrupole interaction strength[7]. The reaction rate with *ortho*-H_2 follows the $E^{1/10}$ scaling law with a fitted interaction strength of $C_5^{eff} = 10.5$ a.u. over more than three orders of magnitude of collision energy (Fig. 4b, dashed blue line).

To confirm that the change in the reaction rate scaling law at low collision energies is only due to the hydrogen molecule's rotational state, we performed additional measurements of the total rate of the He(2^3P_2) + HD reaction (Fig. 4a, grey symbols). The products of the Penning and associative ionization channels include HD^+, HeH^+ and HeD^+, with relative weights of ~90, ~3 and ~7%, respectively, for all the collision energies observed. Because HD is a heteronuclear molecule, the lowest rotational state is $j = 0$, as in the case for *para*-H_2, and the potential surfaces of the two molecules are nearly identical at long range, such that only the reduced mass is changed. Indeed, the resulting energy dependence of the reaction rate for the two isotopologues is nearly identical. The absolute scale of the H_2 reaction rates was normalized according to the thermal rate measurement of He(2^3S_1) + H_2 by Oskam and colleagues[34] in an afterglow study in helium–hydrogen mixtures at 300 K (see Methods). The systematic error in normalization, depicted by the green error bar in Fig. 4b, is much larger than the error in the theoretical C_6^0. For convenience, the relative H_2 rates were therefore scaled up by 22% from the green circle to match the theoretical rate prediction. The rate of He(2^3P_2) + HD is given in arbitrary units and is scaled down by 30% relative to the H_2 measurement.

Importantly, the sharp resonances, which are clearly visible in the reactions with He(2^3S_1)[21,24], disappear in the case of the much faster reactions with He(2^3P_2). This is consistent with the behaviour predicted in the unitary limit, as was recently investigated by Jachymski and colleagues[35]. Below the p-wave barrier energy of 0.04 K for He(2^3P_2) + *ortho*-H_2, the observed rate assumes an approximately constant value. At this energy, there is no centrifugal barrier in the quantum limit as only s-wave scattering can take place and the scaling of the reaction rate becomes consistent with the prediction by the Wigner threshold laws[36–38]. The observed continuous transition from the classical Langevin to quantum behaviour can be used to test recent developments in quantum defect theory, extending it to the non-universal regime[35,39]. Note that our results showing stronger interaction for *ortho*-hydrogen are supported by the earlier spectroscopic measurements of bound van der Waals H_2O–H_2 complexes[40]. The linear scale insets of the reaction rates show the slow changes in the power-law behaviour (Fig. 4).

We have shown that universal Langevin scaling laws can be used to gauge the long-range forces responsible for reactivity in the cold regime, and have experimentally demonstrated that rotationally excited molecules experience stronger long-range attraction, leading to a faster reaction at the low energy range relevant to astrochemical processes.

Methods

Experimental details. The merged beam configuration used consisted of two Even–Lavie supersonic molecular beam valves[41] placed at a relative angle of 10° (Fig. 1). Noble gas mixtures of *para*-H_2/*normal*-H_2/HD were entrained into a straight beam, which was aimed directly at the detection region in a time-of-flight mass spectrometer[42] (TOF-MS). The second beam, which was composed of ^{4}He, was excited to the metastable 2^3S_1 state by a dielectric barrier discharge[43] located directly after the valve. The 20 cm curved magnetic quadrupole guide turned the low-field-seeking metastable helium beam into the straight beam path so that the two beams had a relative angle of zero when they met in the TOF-MS. The relative mean velocity between the beams and the width of their velocity distribution, which was locally decreased by the short opening durations of the Even–Lavie valves, determined the resulting collision energy[22]. Tuning the mean velocities of the beams by seeding the reactants in noble gas mixtures and changing the temperature of the valve allowed the collision energy to be tuned continuously from 300 K to 10 mK.

Collisions of He(2^3P_2) + H_2/HD were realized by exciting He(2^3S_1) in the fully stretched $m = 1$ state to the 2^3P_2 state at 1,083 nm in the reaction volume of the TOF-MS (Fig. 1). A continuous-wave distributed Bragg reflected (DBR) diode laser stabilized by saturated absorption spectroscopy on a helium discharge cell was used for excitation well above the saturation intensity of the transition (0.17 mW cm^{-2})[44], giving a 1:1 population ratio between the two helium states, forming a two-level system. The laser was σ^+ polarized with the quantization, and the quantization axis was defined by a weak magnetic field perpendicular to the beam propagation direction. Excitation therefore occurred along the optical pumping transition between the He(2^3S_1) $m = 1$ state and the 2^3P_2 $m = 2$ state.

The H_2/HD beam was characterized by operating the TOF-MS in a multi-pulsed mode, giving the beam intensity profile at four 4 μs intervals, and the He(2^3S_1) beam was characterized with an on-axis microchannel plate (MCP). He(2^3P_2) was estimated as half He(2^3S_1) due to the 1:1 population ratio between the two. The reaction products were measured in the same way as the H_2/HD beam was characterized, but with the ionizing element turned off. The relative Penning ionization reaction rate at each collision energy of He(2^3S_1) + H_2/HD, measured with the laser off, is given by $k_{2^3S_1}$ in equation (3), where N_n is the measured signal of a species in the nth time interval. The total reaction rate He(2^3P_2) + H_2/HD was measured with the laser on and included both the Penning and associative ionization channels, depicted by $k_{2^3P_2}$, given in equation (4). In both cases the measurement took place over ten time intervals centred at the time when both beams were spatially and temporally overlapped in the TOF-MS.

$$k_{2^3S_1} = \frac{\Sigma_n N_n[H_2^+]}{\Sigma_n(N_n[H_2]N_n[He(2^3S_1)])} \quad (3)$$

$$k_{2^3P_2} = \frac{2\Sigma_n(N_n[H_2^+] + N_n[HeH^+])}{\Sigma_n(N_n[H_2]N_n[He(2^3S_1)])} - k_{2^3S_1} \quad (4)$$

The reaction rates were normalized to an absolute scale according to the thermal rate measurement of He(2^3S_1) + H_2 by Oskam and colleagues[34] in an afterglow study in helium–hydrogen mixtures at 300 K. The thermal rate was calculated with our results, which were all below 300 K, and the rates at higher collision energies by Martin *et al.*[45], which were measured in a crossed beam experiment. The rate for *ortho*-H_2 was determined by subtracting the *para*-H_2 contribution from the *normal*-H_2 measurements.

Samples of *para*-H_2 were prepared by liquefying *normal*-H_2 with liquid helium while in contact with a catalyst of nickel(II) sulfate. The purity of the sample was determined with resonance-enhanced multiphoton ionization (REMPI) followed by detection with the TOF-MS, which indicated that more than 95% of the H_2 was in the $j = 0$ state, compared to 25% in rotationally cold *normal*-H_2. The 3 + 1 REMPI process makes use of the spectroscopically resolved three-photon transition $C^1\Pi_u$, $v = 2 \leftarrow X^1\Sigma_g^+$, $v = 0$ along the R branch at 289.5 nm, followed by a fourth photon that ionizes the molecule[46]. Laser pulses (8 mJ in 10 ns) were generated by a pulsed dye laser (Sirah Cobra-Stretch, pumped by a Spectra Physics Quanta-Ray Pro) and focused by 500 mm lens. The observed rotational state abundance spectrum of H_2 is shown in Supplementary Fig. 2.

Potential energy curve calculation details. The potential energy curves were calculated for the two most symmetric configurations: linear and T-shaped geometries. The potential energy curves for the interaction of He(2^3P) + H_2 in the $^3\Pi$ state for the linear geometry and the $^3B_2$ state for the T-shaped configuration, shown in Fig. 2b, as well as He(2^3S_1) + H_2 in the linear and T-shaped geometries, were obtained with the supermolecular approach using the restricted open-shell Hartree–Fock (ROHF) method followed by spin-unrestricted coupled-cluster calculations with single, double and noniterative triple excitations [UCCSD(T)]. The $^3B_1$ state of the T-shaped geometry was also calculated using this method and is shown in Supplementary Fig. 1. In the ROHF calculations, convergence to the desired excited state (corresponding to the interaction of H_2 with He(2^3P)), was enforced by a suitable rotation of the occupied orbitals. A similar approach[24,47] has already been successfully applied to He(2^3S_1) + H_2. The H_2 bond length was kept fixed at $r = 1.449a_0$.

For the $^3\Sigma$ state of the linear geometry and the $^3A_1$ state of the T-shaped geometry, which are shown in Supplementary Fig. 1, a different approach was used. For these symmetries we obtained the potentials in the spirit of the stabilization method. To this end, we performed standard calculations of the excited states employing linear response theory within the coupled-cluster singles, doubles and linear triple excitations (LR-CC3) and carefully identified states that correspond to the He(2^3P) + H_2 asymptote. This procedure was repeated for a series of basis sets: d-aug-cc-pVTZ/-pVQZ/-pV5Z, yielding very similar results (for example, the well depth of the $^3\Sigma$ potential differs by less than 2.5% between the d-aug-cc-pVQZ and d-aug-cc-pV5Z basis sets). Good convergence with respect to the size of the basis set allows us to assume that the calculated potential energy curves are a decent estimation of the real potentials. The presented interaction potentials are also fairly consistent with results obtained from symmetry adapted perturbation theory extended to open-shell systems[48].

Calculation details for long-range interaction strengths. To compute the isotropic C_6^0 coefficient, the dipole polarizability for H_2 at imaginary and real frequencies was taken from Bishop and Pipin[49], and the polarizability for He(2^3P) was constructed from the sum-over-states expression. The dipole moments of the necessary states and transitions were obtained from multi-reference configuration interaction calculations with single and double excitations (MRCISD) with 27 orbitals in the active space. A doubly-augmented Dunning's d-aug-cc-pV5Z basis set was chosen for the hydrogen and helium atoms in all calculations. The potential calculations used the MOLPRO[50] and DALTON[51] *ab initio* quantum chemistry suites of codes.

Ionization width calculation details. Penning ionization width as a function of the He(2^3P) – H_2 distance was calculated using the *ab initio* Fano–algebraic diagrammatic construction (Fano-ADC) method[52–54] adapted to the decay of triplet excited states. A hole-localization-based configuration selection procedure[52] was used to identify the initial state and final state subspaces within the extended second-order ADC scheme [ADC(2)x]. *Ab initio* calculations were performed using the fully uncontracted cc-pV5Z Gaussian-type basis[55] augmented by 8s4p3d2f1g Kaufmann–Baumeister–Jungen continuum-like diffuse Gaussians[56]. Stieltjes imaging[57] was used for renormalization and interpolation of the Penning matrix elements resulting from the L2 calculations. The Hartree–Fock solution for the ground state of the neutral system was obtained using MOLCAS 7.6 quantum chemistry package[58].

Received 14 April 2015; accepted 25 August 2015; published online 5 October 2015

References

1. Dalgarno, A. in *Molecular Hydrogen in Space* (eds Combes, F. & Pineau des Forêts, G.) 3 (Cambridge Univ. Press, 2000).
2. Brünken, S. *et al.* H_2D^+ observations give an age of at least one million years for a cloud core forming Sun-like stars. *Nature* **516,** 219–221 (2014).
3. Herbst, E. Interstellar processes: *ortho*/*para* conversion, radiative association, and dissociative recombination. *EPJ Web Conf.* **84,** 06002 (2015).
4. Smith, I. W. M. Reactions at very low temperatures: gas kinetics at a new frontier. *Angew. Chem. Int. Ed.* **45,** 2842–2861 (2006).
5. Clary, D. C. Fast chemical reactions: theory challenges experiment. *Annu. Rev. Phys. Chem.* **41,** 61–90 (1990).
6. Herbst, E. Three milieux for interstellar chemistry: gas, dust, and ice. *Phys. Chem. Chem. Phys.* **16,** 3344–3359 (2014).
7. Groenenboom, G. C. & Janssen, L. M. C. in *Tutorials in Molecular Reaction Dynamics* (eds Brouard, M. & Vallance, C.) 392–407 (RSC, 2010).
8. Langevin, P. Une formule fondamentale de théorie cinétique. *Ann. Chim. Phys.* **5,** 245 (1905).
9. Troe, J. *Advances in Chemical Physics* Vol. 82 (eds Baer, M. & Ng, C.-Y.) 485–529 (Wiley, 1992).
10. Dashevskaya, E. I., Litvin, I., Nikitin, E. E. & Troe, J. Rates of complex formation in collisions of rotationally excited homonuclear diatoms with ions at very low temperature: application to hydrogen isotopes and hydrogen-containing. *J. Chem. Phys.* **122,** 184311 (2005).
11. Olkhov, R. V. & Smith, I. W. M. Rate coefficients for reaction and for rotational energy transfer in collisions between CN in selected rotational levels ($X^2\Sigma^+$, $v = 2$, $N = 0$, 1, 6, 10, 15, and 20) and C_2H_2. *J. Chem. Phys.* **126,** 134314 (2007).
12. Ospelkaus, S. *et al.* Quantum-state controlled chemical reactions of ultracold potassium–rubidium molecules. *Science* **327,** 853–857 (2010).
13. Chang, Y.-P. *et al.* Specific chemical reactivities of spatially separated 3-aminophenol conformers with cold Ca^+ ions. *Science* **342,** 98–101 (2013).
14. Marquette, J., Rowe, B. R., Dupeyrat, G., Poissant, G. & Rebrion, C. Ion–polar-molecule reactions: a CRESU study of He^+, C^+, $N+H_2O$, NH_3, at 27, 68 and 163 K. *Chem. Phys. Lett.* **122,** 431–435 (1985).
15. Rowe, B. R., Marquette, J. B., Dupeyrat, G. & Ferguson, E. E. Reactions of He^+ and N^+ ions with several molecules at 8 K. *Chem. Phys. Lett.* **113,** 403–406 (1985).
16. Ni, K.-K. *et al.* Dipolar collisions of polar molecules in the quantum regime. *Nature* **464,** 1324–1328 (2010).
17. Hudson, E., Gilfoy, N., Kotochigova, S., Sage, J. & DeMille, D. Inelastic collisions of ultracold heteronuclear molecules in an optical trap. *Phys. Rev. Lett.* **100,** 203201 (2008).

18. Zahzam, N., Vogt, T., Mudrich, M., Comparat, D. & Pillet, P. Atom–molecule collisions in an optically trapped gas. *Phys. Rev. Lett.* **96,** 023202 (2006).
19. Staanum, P., Kraft, S. D., Lange, J., Wester, R. & Weidemüller, M. Experimental investigation of ultracold atom–molecule collisions. *Phys. Rev. Lett.* **96,** 023201 (2006).
20. Jankunas, J., Jachymski, K., Hapka, M. & Osterwalder, A. Observation of orbiting resonances in $He(^3S_1) + NH_3$ Penning ionization. *J. Chem. Phys.* **142,** 164305 (2015).
21. Henson, A. B., Gersten, S., Shagam, Y., Narevicius, J. & Narevicius, E. Observation of resonances in Penning ionization reactions at sub-kelvin temperatures in merged beams. *Science* **338,** 234–238 (2012).
22. Shagam, Y. & Narevicius, E. Sub-kelvin collision temperatures in merged neutral beams by correlation in phase-space. *J. Phys. Chem. C* **117,** 22454–22461 (2013).
23. Jankunas, J., Bertsche, B. & Osterwalder, A. Study of the $Ne(^3P_2) + CH_3F$ electron-transfer reaction below 1 K. *J. Phys. Chem. A* **118,** 3875–3879 (2014).
24. Lavert-Ofir, E. *et al.* Observation of the isotope effect in sub-kelvin reactions. *Nature Chem.* **6,** 332–335 (2014).
25. Siska, P. E. Molecular-beam studies of Penning ionization. *Rev. Mod. Phys.* **65,** 337–412 (1993).
26. Roberge, W. & Dalgarno, A. The formation and destruction of HeH^+ in astrophysical plasmas. *Astrophys. J.* **255,** 489 (1982).
27. Lique, F., Li, G., Werner, H.-J. & Alexander, M. H. Communication: non-adiabatic coupling and resonances in the $F + H_2$ reaction at low energies. *J. Chem. Phys.* **134,** 231101 (2011).
28. Holmgren, S. L., Waldman, M. & Klemperer, W. Internal dynamics of van der Waals complexes. I. Born–Oppenheimer separation of radial and angular motion. *J. Chem. Phys.* **67,** 4414 (1977).
29. Dubernet, M.-L. & Hutson, J. M. Atom–molecule van der Waals complexes containing open-shell atoms. I. General theory and bending levels. *J. Chem. Phys.* **101,** 1939 (1994).
30. Kirste, M. *et al.* Quantum-state resolved bimolecular collisions of velocity-controlled OH with NO radicals. *Science* **338,** 1060–1063 (2012).
31. Makrides, C. *et al.* Ultracold chemistry with alkali-metal–rare-earth molecules. *Phys. Rev. A* **91,** 012708 (2015).
32. Buckingham, A. D. Molecular quadrupole moments. *Q. Rev. Chem. Soc.* **13,** 183 (1959).
33. Gorin, E. Photolysis of aldehydes and ketones in the presence of iodine vapor. *J. Chem. Phys.* **7,** 256 (1939).
34. Veatch, G. & Oskam, H. Collision processes occurring in decaying plasmas produced in helium–hydrogen mixtures. *Phys. Rev. A* **8,** 389–396 (1973).
35. Jachymski, K., Krych, M., Julienne, P. S. & Idziaszek, Z. Quantum-defect model of a reactive collision at finite temperature. *Phys. Rev. A* **90,** 042705 (2014).
36. Gribakin, G. & Flambaum, V. Calculation of the scattering length in atomic collisions using the semiclassical approximation. *Phys. Rev. A* **48,** 546–553 (1993).
37. Sadeghpour, H. R. *et al.* Collisions near threshold in atomic and molecular physics. *J. Phys. B* **33,** R93–R140 (2000).
38. Wigner, E. On the behavior of cross-sections near thresholds. *Phys. Rev.* **73,** 1002–1009 (1948).
39. Gao, B. Universal model for exoergic bimolecular reactions and inelastic processes. *Phys. Rev. Lett.* **105,** 263203 (2010).
40. Nesbitt, D. J. High-resolution infrared spectroscopy of weakly bound molecular complexes. *Chem. Rev.* **88,** 843–870 (1988).
41. Even, U., Jortner, J., Noy, D., Lavie, N. & Cossart-Magos, C. Cooling of large molecules below 1 K and He clusters formation. *J. Chem. Phys.* **112,** 8068 (2000).
42. Wiley, W. C. & McLaren, I. H. Time-of-flight mass spectrometer with improved resolution. *Rev. Sci. Instrum.* **26,** 1150 (1955).
43. Luria, K., Lavie, N. & Even, U. Dielectric barrier discharge source for supersonic beams. *Rev. Sci. Instrum.* **80,** 104102 (2009).
44. Metcalf, H. J. & van der Straten, P. *Laser Cooling and Trapping* (Springer, 1999).
45. Martin, D. W., Weiser, C., Sperlein, R. F., Bernfeld, D. L. & Siska, P. E. Collision energy dependence of product branching in Penning ionization: $He^*(2^1S, 2^3S) + H_2$, D_2, and HD. *J. Chem. Phys.* **90,** 1564 (1989).
46. Pratt, S. T., Dehmer, P. M. & Dehmer, J. L. Photoionization of excited molecular states. H_2 C $^1\Pi_u$. *Chem. Phys. Lett.* **105,** 28–33 (1984).
47. Hapka, M., Chałasiński, G., Kłos, J. & Żuchowski, P. S. First-principle interaction potentials for metastable $He(^3S)$ and $Ne(^3P)$ with closed-shell molecules: application to Penning-ionizing systems. *J. Chem. Phys.* **139,** 014307 (2013).
48. Hapka, M., Żuchowski, P. S., Szczęśniak, M. M. & Chałasiński, G. Symmetry-adapted perturbation theory based on unrestricted Kohn–Sham orbitals for high-spin open-shell van der Waals complexes. *J. Chem. Phys.* **137,** 164104 (2012).
49. Bishop, D. M. & Pipin, J. Dipole, quadrupole, octupole, and dipole–octupole polarizabilities at real and imaginary frequencies for H, He, and H_2 and the dispersion-energy coefficients for interactions between them. *Int. J. Quantum Chem.* **45,** 349–361 (1993).
50. Werner, H.-J. *et al.* MOLPRO, version 2012.1; http://www.molpro.net
51. Aidas, K. *et al.* The Dalton quantum chemistry program system. *Wiley Interdiscip. Rev.: Comput. Mol. Sci.* **4,** 269 (2014).
52. Averbukh, V. & Cederbaum, L. S. *Ab initio* calculation of interatomic decay rates by a combination of the Fano ansatz, Green's-function methods, and the Stieltjes imaging technique. *J. Chem. Phys.* **123,** 204107 (2005).
53. Gokhberg, K., Averbukh, V. & Cederbaum, L. S. Decay rates of inner-valence excitations in noble gas atoms. *J. Chem. Phys.* **126,** 154107 (2007).
54. Kopelke, S., Gokhberg, K., Averbukh, V., Tarantelli, F. & Cederbaum, L. S. *Ab initio* interatomic decay widths of excited states by applying Stieltjes imaging to Lanczos pseudospectra. *J. Chem. Phys.* **134,** 094107 (2011).
55. Extensible Computational Chemistry Environment Basis Set Database, Version 02/25/04 (Molecular Science Computing Facility, Environmental and Molecular Sciences Laboratory, Pacific Northwest Laboratory).
56. Kaufmann, K., Baumeister, W. & Jungen, M. Universal Gaussian basis sets for an optimum representation of Rydberg and continuum wavefunctions. *J. Phys. B* **22,** 2223–2240 (1989).
57. Langhoff, P. in *Electron–Molecule and Photon–Molecule Collisions* (eds Rescigno, T., McKoy, V. & Schneider, B.) 183 (Plenum, 1979).
58. Aquilante, F. *et al.* MOLCAS 7: the next generation. *J. Comput. Chem.* **31,** 224–247 (2010).

Acknowledgements

The authors thank R. Kosloff and R. Moszynski for discussions as well as O. Tal and D. Rakhmilevitch for advice and help in the generation of *para*-hydrogen. This research was made possible, in part, by the historic generosity of the Harold Perlman family. The authors acknowledge financial support from the European Commission through ERC grant EU-FP7-ERC-CoG 1485 QuCC (Y.S., A.K., E.N.), from the Alexander von Humboldt Foundation (W.S.), from the Lee Family Foundation (R.Y.) and from the UK's Engineering and Physical Sciences Research Council (V.A., R.Y.) through the Career Acceleration Fellowship (award EP/H003657/1) and the Programme Grant on Attosecond Dynamics (award EP/I032517), as well as from the Deutsche Forschungsgemeinschaft through Research Unit 1789 (V.A.).

Author contributions

The experimental work and data analysis were carried out by Y.S., A.K. and E.N. *Ab initio* potential surfaces and interaction strengths were calculated by W.S. The ionization widths were calculated by R.Y. and V.A. All authors contributed to the discussion of experimental results, derivation of the theoretical model and writing of the manuscript.

Additional information

Supplementary information is available in the online version of the paper. Reprints and permissions information is available online at www.nature.com/reprints. Correspondence and requests for materials should be addressed to E.N.

Competing financial interests

The authors declare no competing financial interests.